A filtering method for signal equalization in region-of-interest fluoroscopy

Normand Robert[a)]
Canadian Heart Research Centre, 250 University Avenue, Toronto, Ontario M5H 4E6, Canada

Philip T Komljenovic and J. A. Rowlands
Department of Medical Biophysics, Imaging Research, Sunnybrook and Women's College Health Science Centre, University of Toronto, 2075 Bayview Avenue, Toronto, Ontario M4N 3M5, Canada

(Received 18 June 2001; accepted for publication 5 February 2002; published 12 April 2002)

A method to significantly reduce the exposure area product in fluoroscopy using a pre-patient region-of-interest (ROI) attenuator is presented. The attenuator has a thin central region and a gradually increasing thickness away from the center. It is shown that the unwanted brightening artifact caused by the attenuator can be eliminated by attenuating the low spatial frequencies in the detected image using digital image processing techniques. An investigation of the best image processing method to correct for the presence of the attenuator is undertaken. The correction procedure selected is suitable for use with real-time image processors and the ROI attenuator can be permitted to move during image acquisition. Images of an anthropomorphic chest phantom acquired in the presence of the ROI attenuator using an x-ray image intensifier/video chain are corrected to illustrate the clinical feasibility of our approach. [DOI: 10.1118/1.1470205]

Key words: fluoroscopy, angiography, coronary angiograms, ROI fluoroscopy, equalization

I. INTRODUCTION

Fluoroscopic imaging is the name given to x-ray techniques where video frames are obtained in rapid succession allowing real-time visualization of anatomical structures of interest. Currently, fluoroscopic image frames are acquired using an x-ray image intensifier (XRII), recorded using a video camera and can be digitized to facilitate processing and transmission of the image sequences.

A typical fluoroscopic patient entrance exposure rate is 3 R/min (30 mGy/min skin dose).[1] Interventional procedures such as coronary artery angioplasty and stent placement, catheter ablation, neuroembolization, and transjugular intrahepatic portosystemic shunt placement can require longer fluoroscopy time resulting in high patient exposures.[2–5] These lengthy image guided therapeutic procedures can cause somatic effects such as dermal atrophy and necrosis as well as increase the risk of cancer in patients and physicians.[6]

Thus, there is a great incentive to reduce patient exposure during fluoroscopic procedures. However, XRII fluoroscopic imaging systems are already quantum limited so it is impossible to the reduce patient exposure rate while maintaining the image noise constant. To reduce the exposure rate without creating a negative impact on diagnostic quality, the characteristics of the information needed for diagnosis must be analyzed. For example, in some applications, pulsed fluoroscopy can reduce the mean exposure rate without significant image degradation[7–9] through a reduction in frame rate. As another example, during some interventional procedures, some regions of the image may be more important than other regions which are only needed to provide contextual information. In instances where areas important for diagnosis can be localized to a particular region of the image, a pre-patient region-of-interest (ROI) attenuator can be used to reduce the exposure in less important regions.[10–12]

Rudin *et al.*[10] have demonstrated the benefits of using a ROI attenuator to reduce overall patient exposure during fluoroscopy. A reduction of the input exposure outside the ROI provides the added bonus of improving image quality within the ROI by reducing scattered radiation.[10] Rudin *et al.*[13] have demonstrated that the exposure area product can be decreased by a factor of 5 and the contrast within the ROI improved by a factor of 1.7 without a grid (a factor of 1.3 with a 10:1 grid) by narrowing the fully irradiated field of view from 400 to 79 cm^2.

The approaches developed by Rudin *et al.*[10] and Labbe *et al.*[11] use a ROI attenuator with sharp boundaries. In Rudin's approach, a previously acquired mask image is used to correct for brightening caused by the ROI attenuator so the attenuator cannot be repositioned during fluoroscopic acquisition. Errors in the correction process may cause an artifact in regions of the image onto which the sharp boundaries of the attenuator project. This artifact is not severe so that it can be regarded as a marker useful in localizing the position of the high quality region of the image. Labbe *et al.*[11] have suggested an alternative method where the position of the ROI attenuator is determined by searching for a circular brightening artifact. The method to identify the ROI attenuator position is very computer intensive so the ROI attenuator position has to be fixed during x-ray acquisition. Finally, Sassi *et al.*[12] have proposed a novel approach using a rotating fan beam attenuator. The advantage of their approach is the absence of beam hardening due to the attenuator in the low exposure region of the image.

Our proposed approach to modulating the patient exposure is to use a pre-patient ROI attenuator without sharp

boundaries and correct the resulting image using a digital equalization filter. Thus the effect of the attenuator on the image can be corrected without having to know in advance where its projection is located. The size and position of the high transmission region can vary even during image acquisition and the images can still be corrected and displayed in real time. The key enabling concept is that the pre-patient attenuator is designed to modulate only the lower spatial frequencies of the image so that postprocessing of the digitally acquired images can be performed to hide the attenuator. For example, a high pass spatial digital filter can be used. This approach has the added advantage of eliminating the difficult task of hiding sharp boundary artifacts. This postprocessing also alters the overall appearance of the image resulting in an equalized image having improved display characteristics.

In many x-ray procedures, lower spatial frequencies, which provide large area contrast but contain no significant diagnostic information, cause large variations in signal intensity over the image and can stress the dynamic range of the image display. These low frequency components can make it difficult to visualize small features in both the over and underexposed portions of the image. X-ray equalization, a procedure in which the input exposure spatial distribution is modulated to equalize the exposure to the detector, can be used to remedy this problem. X-ray equalization has been applied to chest radiography[14] resulting in a commercial system known as AMBER[15] and in a prototype system for mammography.[16]

Equalization is a side effect of our approach but is also considered desirable in its own right. In our approach, equalization is done after acquisition to mask the presence of the ROI attenuator. This type of processing does not equalize the signal-to-noise ratio but may improve the display characteristics of the image.

II. METHODS

A. Simulations

Computer simulations were used to model the effect of adding a pre-patient ROI attenuator to clinical angiographic images. The images were acquired on a Philips cardiac angiography systems and were recorded as 512×512 pixel image sequence (8 bit depth) at 15 frames/s on DICOM format cardiology compact disks. The DICOM files were read with the aid of the Papyrus toolkit (University of Geneva). The resulting images were used to investigate various strategies to remove artifacts caused by the ROI attenuator. The original images were compared to the attenuated equalized images visually. Quantitative comparison measures were also developed and used to optimize the equalization process.

1. Attenuator simulation

Figure 1 illustrates the geometry for acquiring clinical angiographic images with the ROI attenuator. The effect of introducing a pre-patient ROI attenuator was simulated with previously acquired angiographic images (having no such attenuator).

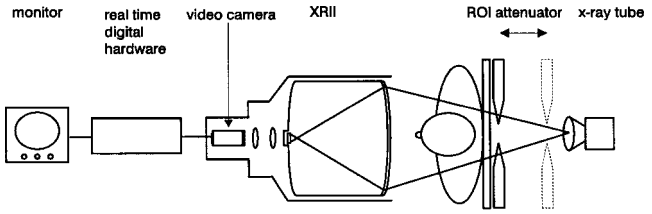

FIG. 1. Angiographic image acquisition geometry. X rays are spatially modulated by a prepatient region of interest attenuator and interact with the patient. The transmitted radiation is recorded via an x-ray image intensifier and video camera combination.

A ROI attenuator having a smooth and circularly symmetric Gaussian shape was defined. The attenuator is a plate of uniform thickness having a Gaussian center milled out. The thickness of the attenuator is given by

$$P(x,y)=1-e^{-(x^2+y^2)/(2(\sigma W)^2)}, \tag{1}$$

where x and y are pixel coordinates, W is the width of the image in pixels, and σ is the width of the Gaussian function in units of image width (a value of 1/2 would correspond to half the image width). The effect of introducing a ROI attenuator into the x-ray beam was calculated by computing the transmission function

$$A(x,y)=e^{-\mu TP(x,y)}, \tag{2}$$

where μT is a dimensionless thickness-attenuation product and $P(x,y)$ is the previously defined thickness function.

The reduction in exposure area product, R, due to the ROI attenuator is plotted as function of σ and μT in Fig. 2 for a fovea located in the center of the field of view.

A Gaussian thickness function was chosen because it has a smooth shape and a limited spatial extent so that the attenuator would mostly affect the low spatial frequency components of the image. [The transmission function $A(x,y)$, could have been defined to be a Gaussian function instead of using $P(x,y)$, a Gaussian thickness profile intermediary. It

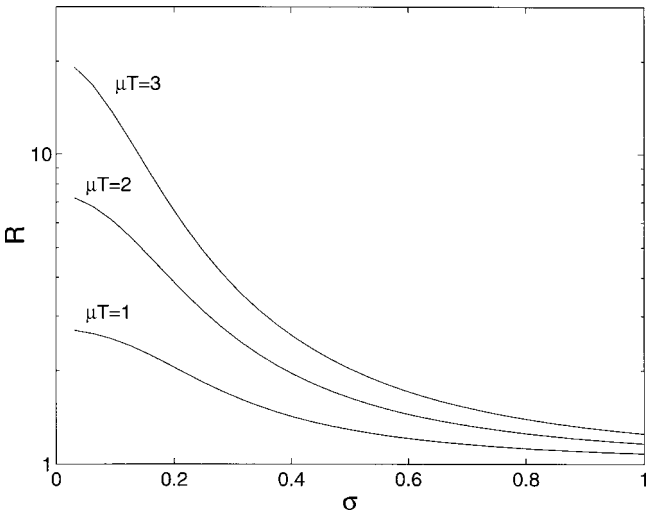

FIG. 2. The reduction in exposure area product, R, as a function of the width of the attenuator σ and thickness μT.

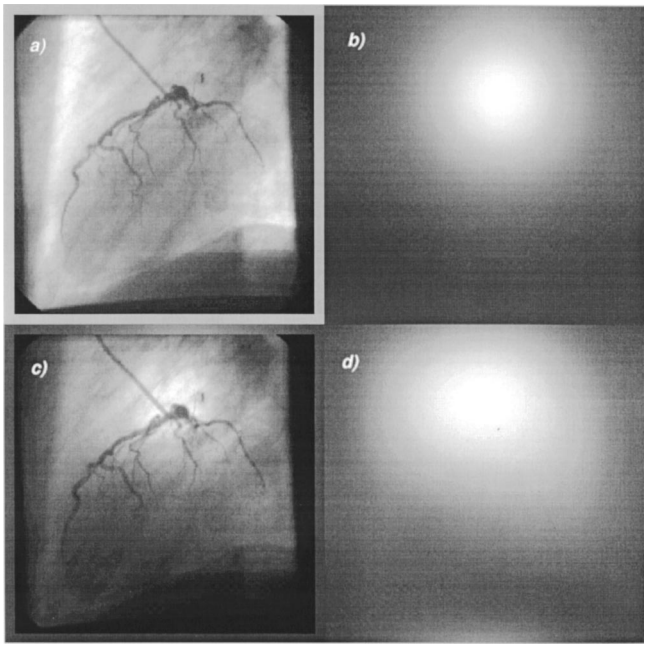

FIG. 3. Simulation of the effect of a ROI attenuator. (a) Original angiographic image frame. (b) The ROI attenuator transmission function, $A(x,y)$. The dark regions corresponds to the highest attenuation. (c) The original frame modified by the application of the attenuator. The ROI attenuator shown in this simulation results in an exposure area product reduction of 5. (d) A blurred version of the attenuated image, $\tilde{A}(x,y)$ shown in (c).

can be shown that our definition also leads to a Gaussian type shape for $A(x,y)$.] Figure 3(a) shows an original image frame $I(x,y)$ from a coronary angiographic cine run. A transmission function with $\mu T=2$ and $\sigma=0.25$ is illustrated in Fig. 3(b). The position of the attenuator was chosen to highlight the left main coronary artery. An attenuated image,

$$I_A(x,y)=I(x,y)A(x,y), \tag{3}$$

is computed and shown in Fig. 3(c). The attenuator causes a noticeable brightening artifact.

2. Equalization method

What is the optimum way to process the data to hide the brightening artifact caused by the ROI attenuator? Equation (3) tells us that accurate removal of the artifact can be achieved by dividing the attenuated image by the transmission function $A(x,y)$. However, the basis of our approach is that $A(x,y)$ is unknown but can be estimated from a low pass version of the ROI attenuated image defined as

$$\tilde{A}(x,y)=I_A(x,y)**G(x,y), \tag{4}$$

where $**$ is a two-dimensional convolution operator and

$$G(x,y)=\frac{1}{2\pi\alpha^2}e^{-(x^2+y^2)/2\alpha^2} \tag{5}$$

is a Gaussian blurring kernel. The image $\tilde{A}$ contains the low frequency information associated with the Gaussian attenuator. Thus, an estimate of the original image is given by

$$\tilde{I}(x,y)=I_A(x,y)/\tilde{A}(x,y). \tag{6}$$

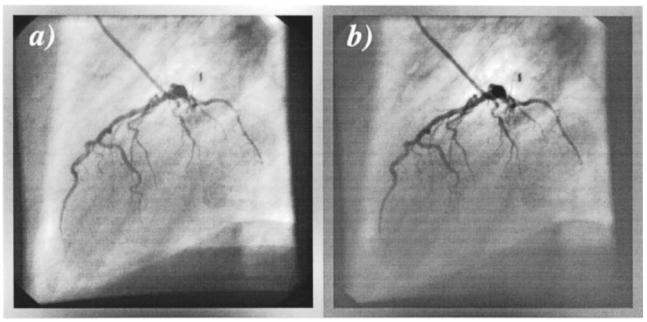

FIG. 4. A comparison of two methods to remove brightening artifacts caused by the ROI attenuator for the frame shown in Fig. 3(c). (a) An equalized image obtained by dividing by $\tilde{A}(x,y)$ (shown in Fig. 3), the blurred version of the original image. (b) An equalized image obtained by subtracting, $\tilde{A}(x,y)$. Both corrected images were obtained using the same value for the Gaussian blurring parameter, α. Methods for choosing suitable α values are given in Sec. III A.

A comparison of Figs. 3(b) and 3(d) which illustrate, respectively, $A(x,y)$ and $\tilde{A}(x,y)$ highlights the similarities between these quantities. Figure 4(a) shows the result of correcting $I_A(x,y)$ [Fig. 3(c)] with $\tilde{A}(x,y)$ [Fig. 3(d)] using Eq. (6). The resulting image, $\tilde{I}(x,y)$, has no visible brightening artifact.

Figure 4(b) shows what happens if one attempts to remove the brightening artifact by subtracting the attenuated image from a blurred version of itself by computing

$$I_{AS}(x,y)=I_A(x,y)-\tilde{A}(x,y). \tag{7}$$

The resulting image, $I_{AS}(x,y)$, exhibits a reduced brightening artifact but it is still noticeable because this approach does not take the effect of the ROI attenuator into account correctly and thus subsequently subtraction was not used, only division.

B. Blurring parameters

The choice of the Gaussian blurring parameter, α, given in Eq. (5), alters the appearance of $\tilde{A}(x,y)$, which affects the attenuated equalized image $\tilde{I}$ computed according to Eq. (6). If too large a value of α is used, $\tilde{A}(x,y)$ will yield a very blurred (uniform) image where the effect of the attenuator is underestimated and dividing $I_A(x,y)$ by $\tilde{A}(x,y)$ results in an image with a residual brightening artifact. If too small a value of α is used, $\tilde{A}(x,y)$ will include features relevant to the diagnosis and these features will be attenuated or removed in $\tilde{I}$.

Our approach rests on the fact that an optimum value of the attenuator blurring parameter α, denoted by $\hat{\alpha}$, can be selected which only affects spatial frequencies in the images that are not important for diagnosis. These frequencies can be attenuated to hide the brightening artifact without decreasing the diagnostic quality of the images. In fact, these images may exhibit better display characteristics.

C. Image comparison criteria

Visual assessment of images processed with different α values could be performed to optimize this parameter. However, it is desirable to develop a quantitative approach to determine the best value of α and how deviations from this optimal value affect the image. An objective (comparison) function providing a measure of agreement that increases as images are more similar as a function of the independent variables μT and σ is required to determine $\hat{\alpha}$.

In order to design a practical comparison function, it is necessary to account for factors that affect the appearance of the x-ray image. For example, the introduction of a uniform thickness attenuator into the x-ray beam would reduce the exposure to the detector if there was no automatic exposure control (AEC) mechanism to compensate for increased x-ray absorption and even with the AEC the correction may not be exact. A comparison of images before and after the introduction of the attenuator (using a simple measure of disagreement between I and $\tilde{I}$) such as the sum of the pixel differences squared would suggest a disagreement. In fact, the images would appear very similar apart from an increase in noise if the attenuated image was rescaled correctly to compensate for its changed signal.

The introduction of a ROI attenuator would reduce the scattered radiation which to a first approximation can be considered to be a signal added to the primary signal. Therefore, a comparison measure that is also insensitive to changes in signal offset would be desirable.

Given an image $I_1(x,y)$, and a second image $I_2(x,y)$ of size $N_2 \times M_2$ pixels, an objective function that provides a measure of similarity between these two images and is insensitive to difference in contrast and brightness can be devised by using the linear correlation coefficient,

$$C = \frac{\Sigma_x \Sigma_y (I_1(x,y) - \overline{I_1})(I_2(x,y) - \overline{I_2})}{\sqrt{\Sigma_x \Sigma_y [I_1(x,y) - \overline{I_1}]^2 \Sigma_x \Sigma_y [I_2(x,y) - \overline{I_2}]^2}}, \tag{8}$$

where

$$\overline{I_1} = \sum_x \sum_y I_1(x,y)/(N_2 M_2),$$

$$\overline{I_2} = \sum_x \sum_y I_2(x,y)/(N_2 M_2).$$

The linear correlation coefficient (LCC) includes normalization factors making it suitable for determining the similarity of a template signal to a target signal when the target signal has been rescaled or an offset has been added to the target signal. The LCC between a target image and template image has a value $C \in [-1.0, 1.0]$, where 1.0 indicates a perfect match with the template within a scaling factor and offset. In other words, if the target image is $I_1(x,y) = aI_2(x,y) + b$ then the LCC operation with the template $I_2(x,y)$ would yield $C = 1.0$ independent of a and b.

There exists several image comparison scenarios for the purpose of optimizing α. The LCC can be used to compare the original image, I, with the attenuated equalized image $\tilde{I}$. This approach seems preferable if one adopts the position that $\tilde{I}$ should look like I as much as possible. The LCC can also be used to compare the low pass image $\tilde{A}$ created during the equalization process and the attenuator profile A. The rationale behind this approach is that under ideal conditions, $\tilde{A}$ will be identical to A within a scaling factor allowing its use to correct for the presence of the ROI attenuator. The following describes how the merit of these approaches is determined.

1. Comparison of the original and attenuated equalized image

The α value that maximizes the LCC between I and $\tilde{I}$ is determined for different angiographic images and attenuators having different values of μT and σ. This image comparison criterion assumes that the best value of α is the one where $\tilde{I}$ most closely resembles I within a scaling factor and offset.

For large values of α, $\tilde{A}$ is very smooth and underestimates the effect of the attenuator causing a residual brightening artifact in $\tilde{I}$. As a result, I and $\tilde{I}$ should differ significantly and C should have a low value. For small values of α, there would be no residual brightening artifact but $\tilde{A}$ now includes signals due to small structures like blood vessels which will cause these structures to be attenuated in $\tilde{I}$. As a result, I should differ significantly once again from $\tilde{I}$ yielding a low C value. For some intermediate $\hat{\alpha}$ value, $\tilde{A}$ should include a brightening artifact but few structures due to the presence of the patient. As a result, differences between I and $\tilde{I}$ will be minimized and C should have a high value. The dependence of $\hat{\alpha}$ on the attenuator characteristics is determined by simulating the effect of attenuators on previously acquired coronary angiograms.

2. Comparison of the attenuator profile and estimated attenuator profile

If the images A and $\tilde{A}$ were identical within a scaling factor, $\tilde{A}$ could be used to undo the effect of the attenuator on the image as described in Eq. (6). To demonstrate this approach, attenuated images are corrected by equalizing with α values that maximize the LCC between A, $\tilde{A}$ for different angiographic images and attenuators having different values of μT and σ.

For small values of α, $\tilde{A}$ should include signals due to structures found in the original image. As a result, A and $\tilde{A}$ should differ and C should have a low value. For large values of α, $\tilde{A}$ should be very blurred and underestimate the effect of the ROI attenuator. As a result, A and $\tilde{A}$ should once again differ and C yields a low value. For some intermediate value $\hat{\alpha}$, $\tilde{A}$ should reproduce the attenuator well but not include patient structures resulting in a large C value. The dependence of $\hat{\alpha}$ on the attenuator characteristics is determined by simulating the effect of attenuators on previously acquired coronary angiograms.

3. Effect of equalization on image features

Instead of comparing the entire images I and $\tilde{I}$ to select $\hat{\alpha}$ values as described in Sec. II C 1, one can evaluate how a particular image feature is preserved in $\tilde{I}$. This approach must be tailored to the imaging task at hand. In the case of angiography one is interested in obtaining information regarding the vessels so other features are generally not of interest. This reasoning has led to the development of digital subtraction angiography (DSA), which isolates iodinated blood vessels by subtracting a previously acquired "mask" image from the frame of interest. DSA is widely used except in the heart where subtraction is not feasible due to the presence of subtraction artifacts caused by cardiac and respiratory motion.

Blood vessel profiles are relatively small features and we will establish that their faithful rendition (within a scaling factor and offset value) does not depend on low spatial frequencies. Simulated vessel cross sections were generated and the cross sections were equalized and compared to the original image. The LCC was used to compare how well the equalized vessel cross sections were reproduced. Hence, a lower limit on the blurring parameter α that still renders the arteries faithfully could be obtained. This value of α was used to equalize angiographic image frames.

D. Effect of the equalization process on signal-to-noise ratio

Given a profile through an image, $L(x)=V(x)+N(x)$, consisting of a vessel profile, $V(x)$, and x-ray noise, $N(x)$, what is the signal-to-noise ratio (SNR) of the vessel and how does the equalization process affect this result? To answer this question we use Wagner's detail SNR definition:[17]

$$\mathrm{SNR}=\left(\frac{\int|S(f_x)|^2df_x}{2[\int W(f_x)|S(f_x)|^2df_x]}\right)^{1/2}, \tag{9}$$

where f_x is the spatial frequency, S is the Fourier transform of the signal, and W is the noise power spectral density.

Let us define the equalized profile $L_E(x:\alpha)=V_E(x:\alpha)+N_E(x:\alpha)$, where $V_E(x:\alpha)$ is the equalized vessel profile, $N_E(x:\alpha)$ is the equalized noise, and the dependency on α is shown explicitly. The SNR of the equalized image is given by

$$\mathrm{SNR}_E(\alpha)=\left(\frac{\int|S_E(f_x:\alpha)|^2df_x}{2[\int W_E(f_x:\alpha)|S_E(f_x:\alpha)|^2df_x]}\right)^{1/2}, \tag{10}$$

where S_E is the Fourier transform of the equalized signal and W_E is the equalized noise power.

Finally, the ratio of the SNR of the original and equalized images is defined

$$\mathrm{SNR}_E(\alpha)/\mathrm{SNR}. \tag{11}$$

In the case of the input SNR, we require

$$S(f_x)=\int V(x)e^{-2\pi if_xx}dx, \tag{12}$$

and

$$W(f_x)=\overline{\int|N(x)|^2e^{-2\pi if_xx}dx}, \tag{13}$$

where the horizontal line indicates that averaging is done over many noise realizations. In the case of the SNR of the equalized image we require

$$S_E(f_x:\alpha)=\int V_E(x:\alpha)e^{-2\pi if_xx}dx. \tag{14}$$

Equalization normalizes the image using a low pass version of the same image. As a result, the equalized noise, N_E, cannot be obtained simply by equalizing noise in isolation from the signal. The equalized noise must be computed by taking the noise and vessel profile components through the equalization process together and subsequently subtracting the equalized vessel profile V_E. Thus, $N_E(x)=L_E(x)-V_E(x)$, where L_E is the equalized image (noise and vessel profile). The equalized noise power is given by

$$W_E(f_x:\alpha)=\overline{\int|L_E(x:\alpha)-V_E(x:\alpha)|^2e^{-2\pi if_xx}dx}. \tag{15}$$

E. X-ray apparatus

X-ray images of phantoms were obtained to quantitatively investigate the ROI equalization fluoroscopy approach. A Rando chest phantom (Phantom Laboratory, Salem, NY) was imaged with a 6 French catheter impregnated with iodine (Omnipaque, Winthrop) secured to the anterior surface of the phantom. Digital images were acquired at 70 kVp without a grid using an XRII–video camera combination. A ROI attenuator, having a Gaussian profile, was built using plaster of paris. Unlike the attenuator described in the simulation studies, the plaster attenuator has nonzero thickness in its thinnest part to facilitate its construction and make it less fragile. A small ion chamber was used to obtain the transmission characteristics of the attenuator.

The minimum thickness of the ROI attenuator was 5 mm resulting in 75% transmission of x rays. The maximum thickness of the attenuator was 25 mm resulting in a 21% transmission of radiation. The tube current was increased while keeping the tube voltage constant in the presence of the ROI attenuator so that the entrance exposure to the patient measured with an ion chamber at the thinnest point of the attenuator would match the exposure with no attenuator making a comparison of the images in that region more fair.

The distance of the attenuator from the x-ray source can be varied to change the projected size of the high exposure region. In the position used for this experiment, the phantom has a σ value of 0.2. The value of μT is 1.6 and the overall reduction in exposure area product is 2.9.

III. RESULTS AND DISCUSSION

A. Modeling results

Equalized images obtained from the three optimization methods for selecting the best α values are presented. The

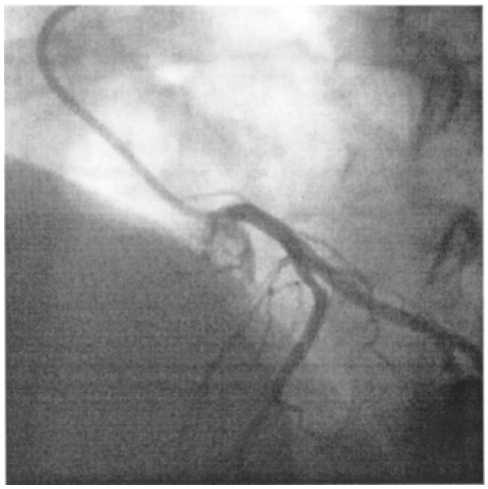

FIG. 5. Original frame used to optimize the value of the equalization parameter α.

first approach is based on a comparison of the equalized image with the original, the second involves a comparison of the attenuator profile and the estimated attenuator profile, and the third is based on an analysis of the effect of equalization on the vessel cross section. Figure 5 shows the original image used for the simulations. This image frame was selected from a clinical cine run showing the coronary arteries of the left side of the heart.

In Fig. 6, the image shown in Fig. 5 is modified with ROI attenuators having four combinations of μT and σ values. Three methods to optimize the value of α were applied to these image frames.

Figure 7 shows what happens if a ROI attenuated image is processed with poorly selected α values. Figure 7(a) was obtained by equalizing with a very small α value resulting in enhancement of the vessel edges accompanied by brightening of structures near the vessel (halo effect). The effect of small α values on the vessel profile is further discussed in Sec. III A 3. Figure 7(b) shows how the use of large α values results in an image where the fovea is quite noticeable.

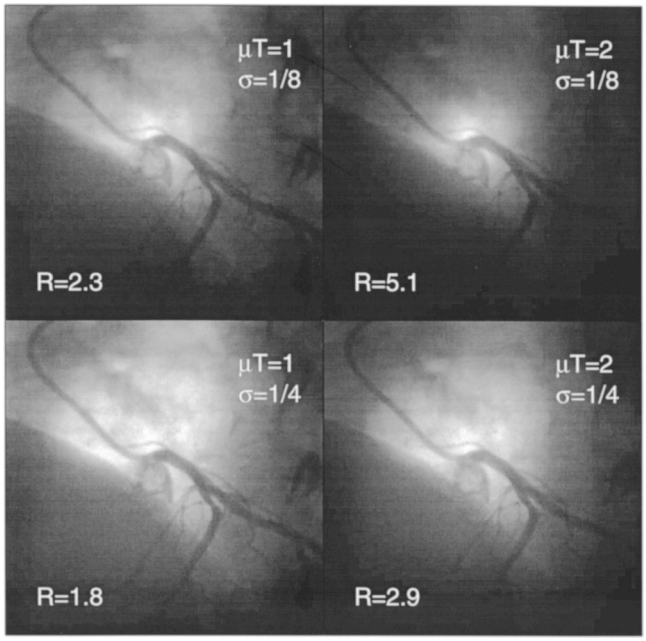

FIG. 6. Images obtained by applying simulated ROI attenuators having different width values, σ, and thicknesses, μT, to the same cine frame. R values indicate the exposure area product reductions.

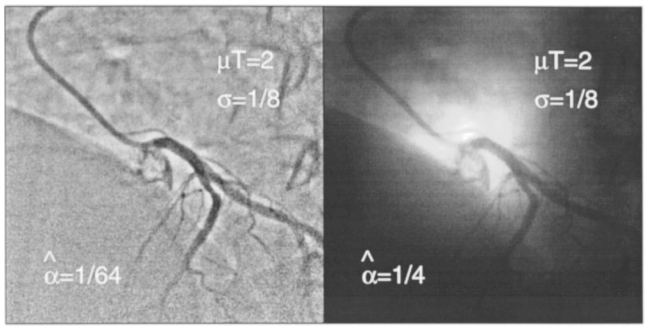

FIG. 7. Examples of images processed to hide the presence of the ROI attenuator. (a) Image equalized with a small α value causing alteration of the vessel profile (edge enhancement). (b) Image equalized with a large α value resulting in a residual brightening artifact revealing the presence of the attenuator.

1. Comparison of the original and attenuated equalized images

In this approach, α values that maximize the similarity between $\tilde{I}$ and I according to the LCC criterion are computed. Values of $\hat{\alpha}$ as a function of μT and σ are shown in Fig. 8(b) and corresponding optimum LCC values are shown in Fig. 8(a). Each data point is a mean value obtained by repeating the optimization procedure on 14 single frames selected from different cine runs.

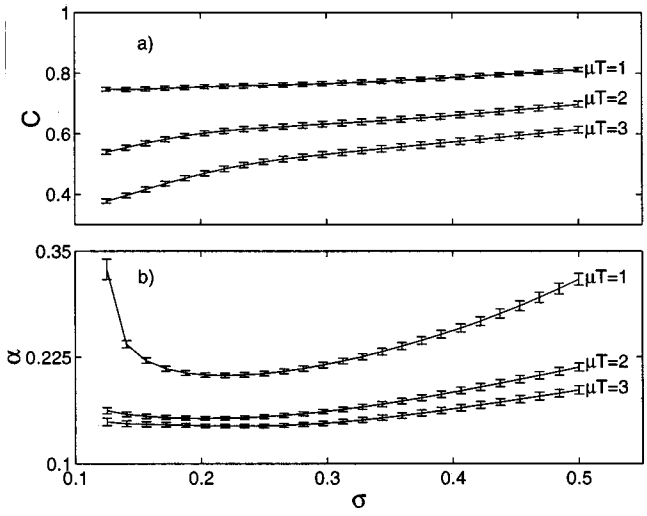

FIG. 8. (a) The optimum linear correlation coefficient, C, a measure of agreement between the original and attenuated equalized images as a function of attenuator thickness, μT, and size σ obtained by finding the values of the filtering parameter, α, yielding the highest C values. (b) The corresponding optimized α values. The error bars in both graphs are the standard errors of the mean.

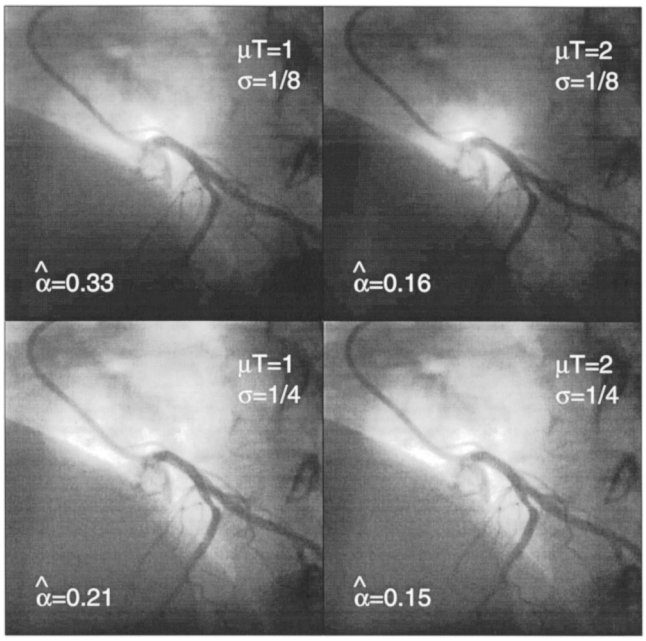

FIG. 9. Equalized images obtained for four combinations of ROI attenuator sizes σ and ROI attenuator thicknesses μT. Each equalized image, $\tilde{I}$, is obtained by dividing the attenuated image by a Gaussian blurred version of itself. In each instance, the blurring parameter $\hat{\alpha}$ was selected to provide optimum agreement between the original and attenuated equalized images in Fig. 8. Residual brightening of the image is noticeable especially for the smaller ROI and thinner attenuator. The exposure area product reductions are the same as in Fig. 6.

An example of some attenuated images equalized using optimal α values given in Fig. 8 are shown in Fig. 9. For a given σ, there exists an $\hat{\alpha}$ value that attenuates the low frequency modulation due to the ROI attenuator and yet transmits most of the high frequency components in the original image. The optimal blurring parameter $\hat{\alpha}$ increases with σ for mid to large σ values because as the attenuator becomes bigger, only the very lowest spatial frequencies need to be attenuated in order to provide a good estimate of A.

In the case of the thin and small ROI attenuator sizes shown in the upper left frame of Fig. 9, the relationship is reversed, $\hat{\alpha}$ increases with decreasing σ. The LCC optimization treats all pixels equally. As the ROI becomes very small this optimization finds that it is better to reproduce the signal accurately in the periphery which occupies a large fraction of the images than it is to remove the brightening artifact which occupies a small region. The best way to reproduce the image in the periphery is to perform little or no equalization; hence the large $\hat{\alpha}$ value. As the ROI becomes larger, the best α is a compromise that would reproduce the signal well both in the high transmission region and the periphery.

All equalized images provide a good visual rendition of the arteries. However, the limitations of a comparison criterion based on the agreement between I and $\tilde{I}$ are highlighted in the case of smaller and thinner attenuators. The calculated optimum α values are too large, permitting some residual brightening to remain in the image.

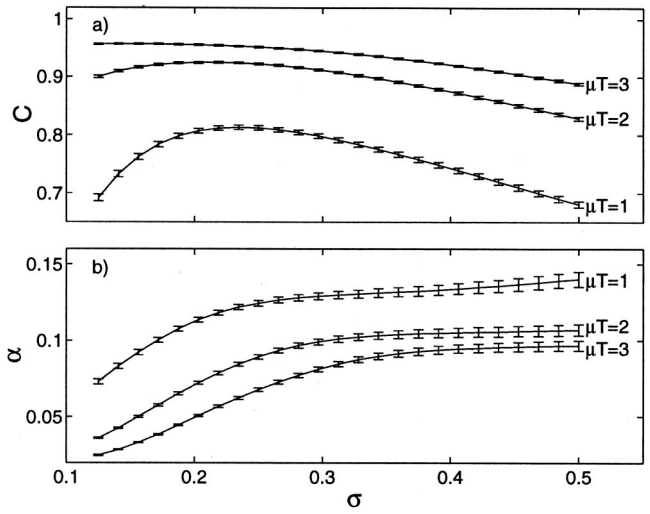

FIG. 10. (a) The linear correlation coefficient value, C, a measure of agreement between the attenuator profile, A, and transmission estimate, $\tilde{A}$, as a function of attenuator thickness, μT, and size, σ, obtained by finding the values of the filtering parameter, α, yielding the highest C values. (b) The corresponding $\hat{\alpha}$ values. The error bars in both graphs are the standard errors of the mean.

2. Comparison of the attenuator and estimated attenuator profiles

In this approach, the α value that maximizes the similarity between $\tilde{A}$ and A is computed based on the LCC criterion. Figure 10(a) shows the dependence of C on attenuator size and thickness while Fig. 10(b) shows the dependence of these $\hat{\alpha}$ values on these same parameters.

The data were obtained by repeating the optimization for various attenuator sizes and thicknesses on single frames from the same 14 cine runs used in Sec. III A 1. The observed trends are as expected. Larger size attenuators can be estimated by a very blurred version of the original frame, so $\hat{\alpha}$ is very large. The effect of a thin attenuator on the image is less noticeable and can be estimated using larger $\hat{\alpha}$ values which are less effective in equalizing the image. Examples of images equalized using $\hat{\alpha}$ values given in Fig. 10 for various values of σ and μT are shown in Fig. 11. The effect of applying the equalization procedure to unattenuated frames using the same $\hat{\alpha}$ values as shown in Fig. 11 is illustrated in Fig. 12 for comparative purposes. This approach results in equalized images for which there is no residual brightening artifacts for all attenuator sizes and thicknesses. The arteries are also well reproduced.

3. Effect of equalization on image features

The effect of equalization on the shape of a vessel profile was determined as a function of α. Figure 13 shows how the original vessel cross section having a diameter d (solid line) is reproduced as the value of the filter parameter α is changed. If $\alpha > d$, the vessel cross section is well reproduced. Knowing the diameter of the largest coronary arteries (6 mm), typical field of view of an XRII (18 cm), and geometric magnification (1.2) we can determine that values of

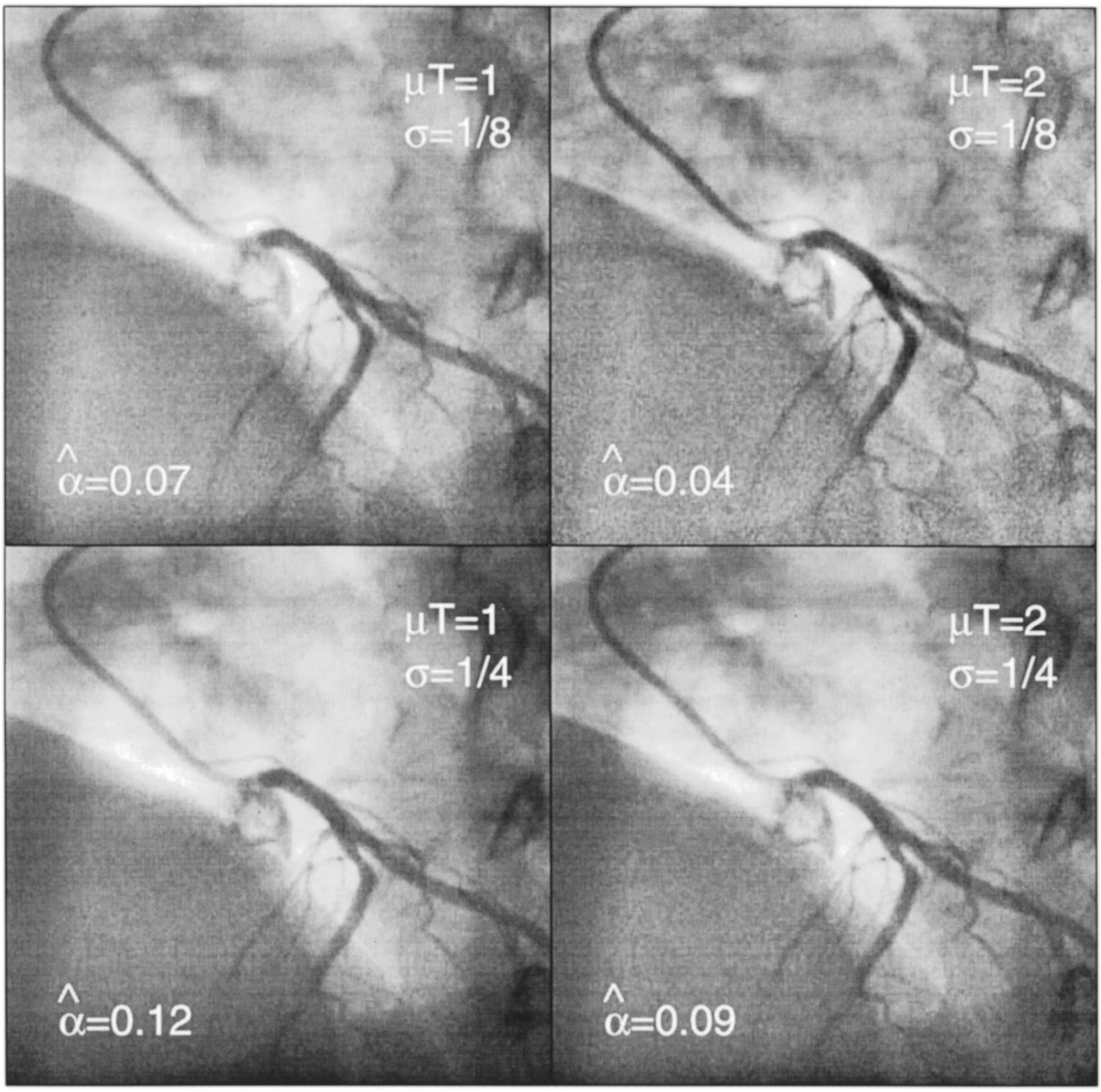

FIG. 11. Equalized images obtained for four combinations of ROI attenuator sizes σ and ROI attenuator thicknesses μT. Each attenuated equalized image, $\tilde{I}$, is obtained by dividing the attenuated image by a Gaussian blurred version of itself. In each instance, the blurring parameter α was selected to provide optimum agreement between the ROI attenuator profile A and ROI transmission estimate $\tilde{A}$ using data shown in Fig. 10. The exposure area product reductions are the same as in Fig. 6. The ROI attenuator profile is well masked in all cases.

$\alpha > 1/20$ of the field of view are adequate to avoid altering the vessel cross section of even the larger vessels.

This approach suggests that smaller values for α can be used when one tailors the equalization process to reproduce a small feature in the image such as coronary blood vessels.

B. Effect of the equalization process on SNR

The SNR of a vessel profile with Poisson noise was calculated using Eq. (9) before and after the equalization process. Figure 14 shows the $\mathrm{SNR}_E(\alpha)/\mathrm{SNR}$ ratio as a function of α expressed in units of vessel diameter d. For very large α, the equalization process is equivalent to dividing the whole image by a scalar quantity which rescales the noise and signal in an identical fashion. Therefore, the SNR ratio becomes close to one. As α is decreased, the contribution of higher spatial frequencies having lower SNR values becomes more significant and causes a reduction in the ratio. However, for $\alpha > d$ this analysis suggests a negligible drop in the SNR ratio due to equalization. It is important to note that the performance of the observer and display system is not taken into account in this analysis. We expect that visualization of vessels will be improved through equalization by allowing the simultaneous display of vessels in bright and dark re-

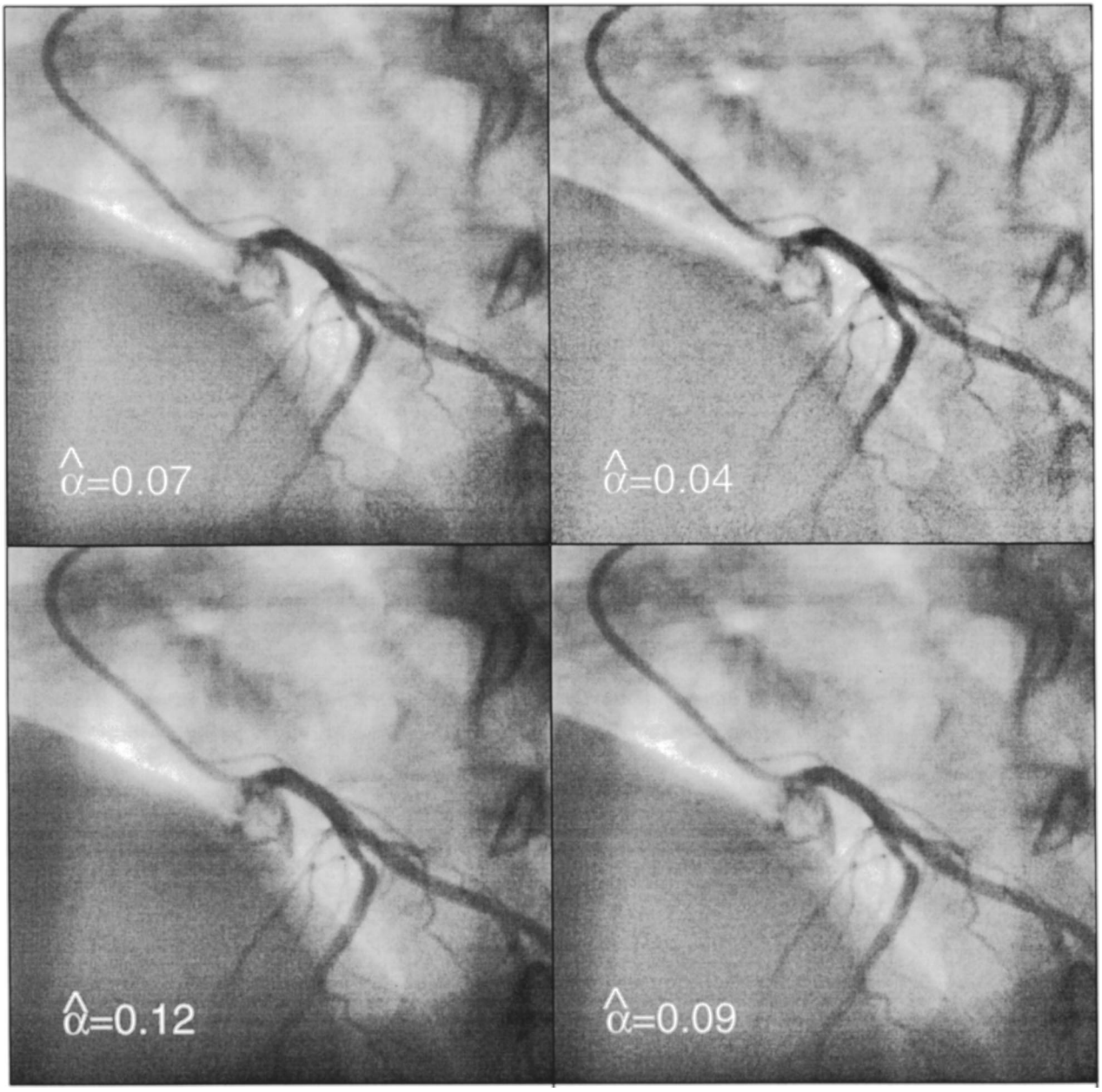

FIG. 12. Equalized images obtained for the same filtering parameter value as shown in Fig. 11 but without simulation of the effect of ROI attenuators.

gions of the image with increased contrast. Thus, the performance of the observer is expected to be improved.

C. X-ray experiments

Figure 15 illustrates the results obtained when applying our ROI equalization approach to an anthropomorphic x-ray chest phantom. The phantom was oriented to reproduce a caudal LAO 60° view. Figure 15(a) shows an image frame of the phantom. Some artifacts in x-ray images related to the fact that the phantom is made up numerous slices were hidden by acquiring a caudal view in which the x rays are incident to the slices at a 60° angle. Figure 15(b) shows the phantom image after applying the equalization correction with $\alpha = 0.04$. The phantom image following the introduction of the pre-patient ROI attenuator is shown in Fig. 15(c). The equalized attenuated image is shown in Fig. 15(d). This image has a similar appearance to Fig. 15(b) indicating the brightening artifacts from the ROI attenuator are no longer visible. There is a noticeable increase in noise in the periphery of the equalized attenuated frame due to the lower x-ray exposure in these regions. Variations in digitized values of pixels due to noise in the low transmission region following equalization can be greater than variations due to signal in the ROI. Therefore, the window and level settings used to display these images must be chosen to optimally show the image within the ROI as was done in Fig. 15(d).

If equalized image frames are shown in sequence, the motion sensitive human visual system may be distracted by the changing pattern of noise in the low transmission region.

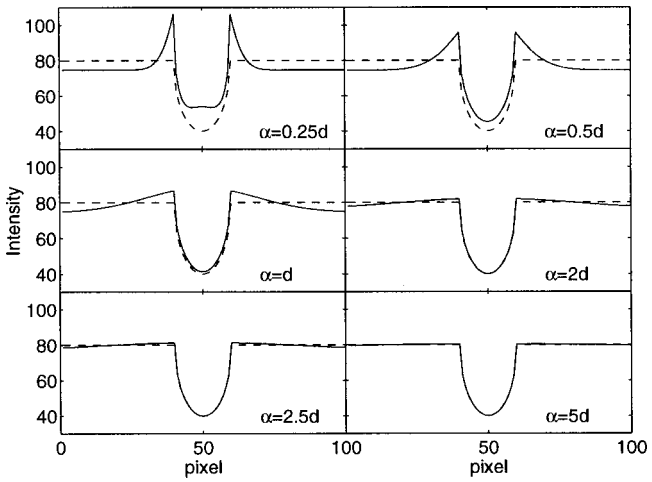

FIG. 13. The original vessel cross sections (dotted line) as well as cross sections obtained following equalization (solid lines) with various values of α expressed in units of vessel diameter. The equalized profile has been normalized to overlap with the original profile.

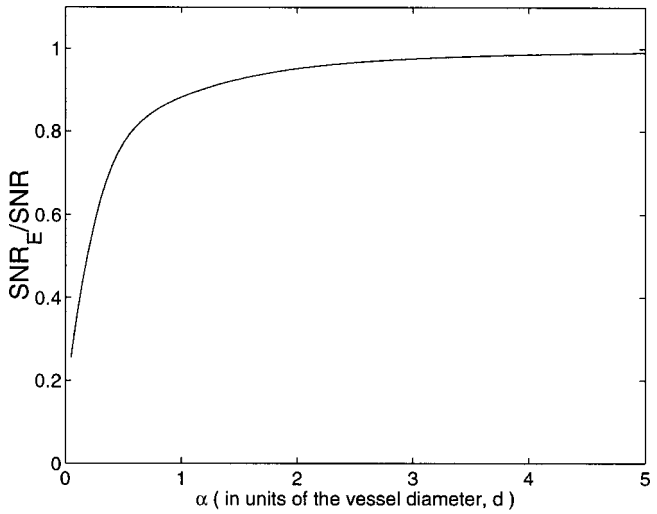

FIG. 14. A graph of the signal-to-noise ratios of a simulated vessel cross section with Poisson noise after and before equalization, SNR_E/SNR, as a function of the equalization parameter α.

A simple noise reduction method is introduced to illustrate the possibility of overcoming this problem in ROI fluoroscopy. A new image, $\tilde{I}''$, is created by combining $\tilde{I}'$, a blurred version of $\tilde{I}$ and $\tilde{I}$ in a spatially dependent manner.

In the high transmission region of the ROI, the transmission estimate, $\tilde{A}$, has a larger value; in the low transmission region, $\tilde{A}$ has a smaller value. Thus, $\tilde{A}$ can be used to weight the relative contribution of $\tilde{I}$ and $\tilde{I}'$ such that $\tilde{I}''$ is composed

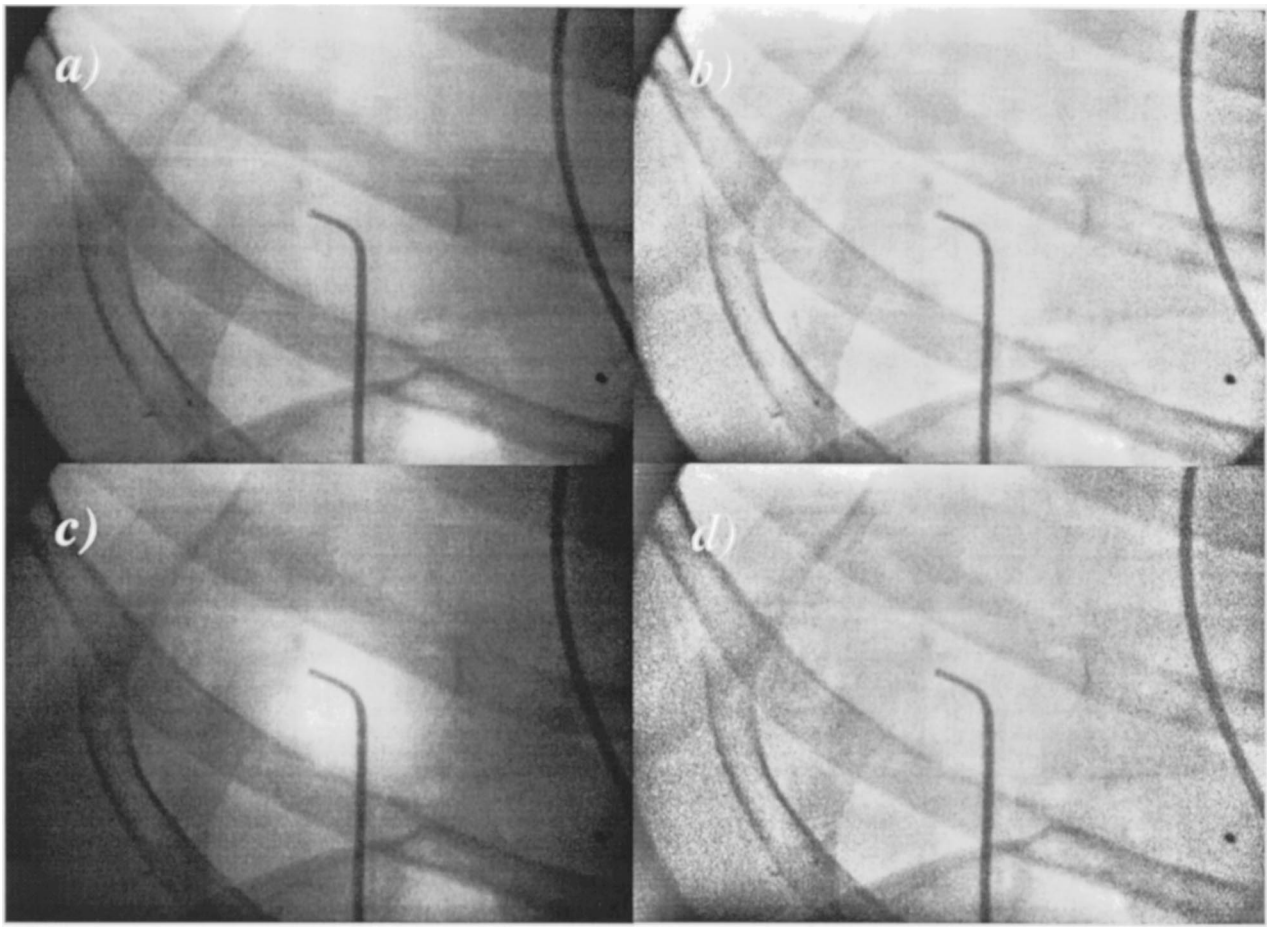

FIG. 15. Digitized frames of an anthropomorphic x-ray phantom used to demonstrate ROI fluoroscopy. (a) The original frame. (b) The same frame as in (a) following equalization. (c) A frame acquired with the ROI attenuator resulting in an exposure area product reduction of 2.9. (d) The same frame as in (c) following equalization.

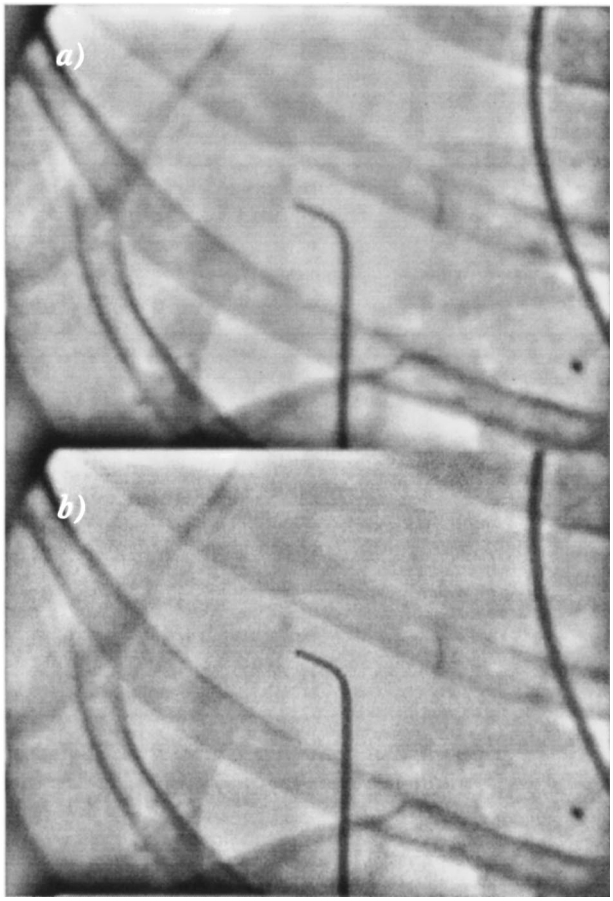

FIG. 16. A scheme to reduce noise in the periphery of the images. (a) A blurred version of the attenuated equalized image, $\tilde{I}'$. (b) A noise reduced equalized image, $\tilde{I}''$, obtained by performing a spatially varying weighted sum of the blurred image in (a) and $\tilde{I}$ shown in Fig. 15(d) where the weighting function is the transmission estimate, $\tilde{A}$. This approach results in more image blurring in the low transmission regions of the image and little or no blurring within the ROI.

mostly of $\tilde{I}$ in the high transmission region and $\tilde{I}'$ outside this region.

Thus, the noise reduced image can be defined as

$$\tilde{I}''(x,y)=\eta\tilde{I}(x,y)+(1-\eta)\tilde{I}'(x,y), \tag{16}$$

where $\tilde{I}'(x,y)=\tilde{I}(x,y)^{**}B(x,y)$, $B(x,y)$ is a Gaussian blurring kernel and

$$\eta=\frac{\tilde{A}(x,y)-\min_{x,y}[\tilde{A}(x,y)]}{\max_{x,y}[\tilde{A}(x,y)]-\min_{x,y}[\tilde{A}(x,y)]} \tag{17}$$

is used to weight the relative contribution of $\tilde{I}$ and $\tilde{I}'(x,y)$ in the output image. An image pair filtered according to Eq. (16) and by computing $\tilde{I}'(x,y)$ using a blurring kernel with $\alpha=2$ pixels is shown to demonstrate the merit of spatially dependent filtering.

If the image is blurred uniformly as shown in Fig. 16(a), noise in the periphery of the frame is less noticeable than in Fig. 15(d) but the catheter is also blurred. Application of the spatially variant filter described in Eq. (16) is shown in Fig. 16(b). The spatially variant blurring results in an image exhibiting less noise yet the sharp appearance of the catheter is maintained.

IV. SUMMARY AND CONCLUSIONS

We have investigated a novel ROI attenuator approach to reducing dose during fluorographic procedures using simulations performed with coronary angiograms. We have described how image equalization can be used to hide brightening artifacts caused by the attenuator. This approach results in a correction where knowledge of the position of the ROI attenuator is not required and where the attenuator position can be changed even during acquisition.

We have illustrated three optimization criteria for choosing the filtering parameter α: (1) A comparison of I and $\tilde{I}$ yielding a larger estimate of α which alters the attenuated image the least but can yield residual brightening artifact, especially for small fovea sizes. (2) A comparison of A and $\tilde{A}$ which produces intermediate α values. This method yields excellent results over a wide range of attenuator thicknesses and widths providing better removal of brightening artifacts. (3) A selection of α based on how it affects a feature of interest in instances where the maximum size of the said feature is known *a priori*. In such instances, the effect of the equalization process can be assessed on representative depictions of the feature of interest as was done for coronary arteries. If the object of interest is small, this approach will produce images that are greatly equalized.

It was shown that the equalization processes effectively hides artifacts caused by the ROI attenuator and does not significantly degrade the signal-to-noise ratio of a vessel. In fact, these images have better display characteristics than nonequalized images allowing small details to be rendered more uniformly over both the low and high exposure regions of the image. Applying these concepts in an x-ray phantom experiment shows that this approach can work in a clinical setting.

Image equalization involves filtering operations that must be performed in real time to be clinically useful. A variation of the method presented in this paper has been implemented on a real time image processor [XRE/Analogic Corp (Boston, MA)] which can be used to equalize 30 512×512 pixel frames per second.[18]

For coronary angiography, our simulations suggest that the simplest approach to choosing the filtering parameter α is to select the smallest value that still shows vessels well. For applications other than coronary angiography where some intermediate spatial frequencies are considered important for diagnosis, α values resulting in less aggressive equalization should be used.

ACKNOWLEDGMENT

This work is supported by a grant from the Canadian Institute for Health Research formerly known as the Medical Research Council of Canada.

[a]Electronic mail: robertn@chrc.net

[1] J. Bushberg, J. S. E. Leidholdt, and J. Boone, *The Essential Physics of Medical Imaging* (Williams and Wilkins, 1994).
[2] J. Cusma, M. Bell, M. Wondrow, T. Taubel, and D. Holmes, ''Real-time measurement of radiation exposure to patients during diagnostic coronary angiography and percutaneous interventional procedures,'' J. Am. Coll. Cardiol. **33**, 427–435 (1999).
[3] L. Rosenthal *et al.*, ''Predictors of fluoroscopy time and estimated radiation exposure during radiofrequency catheter ablation procedures,'' Am. J. Cardiol. **82**, 451–458 (1998).
[4] L. Wexler, ''Cardiac diagnostic and interventional procedures,'' in *A Categorical Course in Physics. Physical and Technical Aspects of Angiography and Interventional Radiology*, edited by S. Balter and T. B. Shope, (RSNA, Chicago, 1995).
[5] B. Berthelsen and A. Cederblad, ''Radiation dose to patient and personnel involved in embolization of intercerebral arteriovenous malformations,'' Acta Radiol. **32**, 492–497 (1991).
[6] L. Wagner, B. Archer, and A. Cohen, ''Management of patient skin dose in fluoroscopically guided interventional procedures,'' J. Vasc. Interv. Radiol. **11**, 25–33 (2000).
[7] P. H. Brown, R. D. Thomas, P. J. Silberberg, and L. M. Johnson, ''Optimization of a fluoroscope to reduce radiation exposure in pediatric imaging,'' Pediatr. Radiol. **30**, 229–235 (2000).
[8] R. J. Hernandez and M. Goodsitt, ''Reduction of radiation dose in pediatric patients using pulsed fluoroscopy,'' Am. J. Roentgenol. **167**, 1247–1253 (1996).
[9] M. Scanavacca, A. d'Avila, J. Velarde, J. Reolao, and E. Sosa, ''Reduction of radiation exposure time during catheter ablation with the use of pulsed fluoroscopy,'' Int. J. Cardiol. **63**, 71–74 (1998).
[10] S. Rudin and D. Bednarek, ''Region of interest fluoroscopy,'' Med. Phys. **19**, 1183–1189 (1992).
[11] M. S. Labbe, M. Y. Chiu, M. S. Rzeszotarski, A. R. Bani-Hashemi, and D. L. Wilson, ''The x-ray fovea, a device for reducing x-ray does in fluoroscopy,'' Med. Phys. **21**, 471–481 (1994).
[12] S. A. Sassi and A. J. Britten, ''Moving segments region of interest attenuator for x-ray fluoroscopy,'' Med. Phys. **26**, 19–26 (1999).
[13] S. Rudin and D. R. Bednarek, ''Spatial shaping of the beam: Collimation, grids, equalization filters, and region of interest fluoroscopy,'' in Ref. 4.
[14] D. B. Plewes and E. Vogelstein, ''A scanning system for chest radiography with regional exposure control: Practical implementation,'' Med. Phys. **10**, 655–663 (1983).
[15] H. Vlasbloem and L. Kool, ''AMBER: a scanning multiple-beam equalization system for chest radiography,'' Radiology **169**, 29–34 (1988).
[16] J. M. Sabol, ''A scan-rotate geometry for efficient equalization mammography,'' Med. Phys. **24**, 137 (1997).
[17] R. F. Wagner, ''Decision theory and the detail signal-to-noise ratio of Otto Schade,'' Photograph. Sci. Eng. **22**, 41–45 (1978).
[18] J. A. Rowlands and P. M. Rieppo, ''Region of interest fluoroscopy with dynamic filtering,'' Radiology (supplement) **189**, 216 (1993).